Applied Radiation and Isotopes 100 (2015) 38–42

Contents lists available at ScienceDirect

Applied Radiation and Isotopes

journal homepage: www.elsevier.com/locate/apradiso

Application of a semi-empirical model for the evaluation of transmission properties of barite mortar

Josilene C. Santos [a], Alessandra Tomal [b,*], Leandro Mariano [a], Paulo R. Costa [a]

[a] Instituto de Física da Universidade de São Paulo, Cidade Universitária, Rua do Matão Travessa R .187, CEP 05508-090 São Paulo, Brazil
[b] Instituto de Física Gleb Wataghin, Universidade de Campinas, Cidade Universitária Zeferino Vaz Barão Geraldo, Rua Sérgio Buarque de Holanda, 777, CEP 13083-859 Campinas, SP, Brazil

HIGHLIGHTS

- Barite mortar attenuation curves using X-ray spectra were calculated.
- Optimized thickness of protective barrier was estimated.
- An optimized model considers the energy spectra for protective barrier calculation.

ARTICLE INFO

Article history:
Received 30 July 2014
Received in revised form
19 December 2014
Accepted 7 January 2015
Available online 8 January 2015

Keywords:
Shielding barriers
X-ray Spectrometry
Solid state detector

ABSTRACT

The aim of this study was to estimate barite mortar attenuation curves using X-ray spectra weighted by a workload distribution. A semi-empirical model was used for the evaluation of transmission properties of this material. Since ambient dose equivalent, $H^*(10)$, is the radiation quantity adopted by IAEA for dose assessment, the variation of the $H^*(10)$ as a function of barite mortar thickness was calculated using primary experimental spectra. A CdTe detector was used for the measurement of these spectra. The resulting spectra were adopted for estimating the optimized thickness of protective barrier needed for shielding an area in an X-ray imaging facility.

1. Introduction

Shielding calculations for medical X-ray imaging facilities are currently based on methods recommended by National Council on Radiation Protection and Measurements (NCRP report 147) (NCRP, 2004). This publication presents physical and operational parameters to be considered in the selection of shielding materials and it establishes modern fundamentals for calculating thicknesses of barriers to be adopted for protecting diagnostic X-ray imaging facilities. This publication uses Archer's model for calculation of transmission curves of shielding materials (Archer et al., 1994) and the workload distributions obtained in US X-ray imaging facilities (Simpkin, 1996). However, NCRPs recommendations are based on data obtained from air kerma measurements, which do not take into account the direct spectral distribution of the X-ray beam transmitted by the protective material. The NCRP data considers different beam qualities, since different applied voltages in use in diagnostic X-ray beams were used, but these data are limited on the representation of the transmitted X-ray spectra. Furthermore, the original model for the evaluation of the transmission curves of the shielding material is presented using the quantity air kerma (Archer et al., 1994), which does not comply to modern requirements which adopt the quantity ambient dose equivalent ($H^*(10)$) to represent the shielding design goals and environmental monitoring (IAEA, 2014). Ambient dose equivalent, $H^*(d)$, at a point of radiation field, is the dose equivalent that would be produced by the corresponding expanded and aligned field in the ICRU sphere at a depth, d, on the radius opposing the direction of aligned field (ICRU, 1998). For penetrating radiation with $d=10$ mm, this is $H^*(10)$.

The transmission curves of different shielding materials presented in NCRP report 147 cover a large sort of materials commonly used for shielding propose, such as lead, concrete, gypsum wallboard, steel and others. However, the report does not present transmission data for barite mortar, which is a material widely used for shielding proposes in many countries (Akkurt et al., 2006; Esen and Yilmazer, 2010; Okkalides, 1991). Some authors studied barite mortar transmission properties for diagnostic X-rays energy range. These data were obtained by computational methods (Hoff

* Corresponding author.
E-mail addresses: josilene@usp.br (J.C. Santos), atomal@ifi.unicamp.br (A. Tomal), lean.mariano@gmail.com (L. Mariano), pcosta@if.usp.br (P.R. Costa).

http://dx.doi.org/10.1016/j.apradiso.2015.01.007
0969-8043/

and Firmino, 2007; Hoff et al., 2009) or experimentally by measurements of transmitted air kerma by an ionizing chamber (Costa and Yoshimura, 2011; Ling et al., 2013). Li et al. (2012) also applied a similar method for X-ray spectra typically used in mammography imaging facilities using Monte Carlo simulations. McCaffrey et al. (2009) also used Monte Carlo methods for studying shielding optimization applying non-lead bilayers.

Some of these works present evaluations of the transmission properties of conventional barite mortar or mortars composed of different barite aggregates, but do not present the results in terms of a radiometric quantity, nor do they take into account the effect of these materials on transmitted X-ray spectra. Moreover, these authors do not present correlations between the transmission properties and the workload commonly found in real X-ray imaging facilities (Santos and Costa, 2014). They also used simulated X-ray beams, not measured radiation spectra with radiation qualities commonly found in diagnostic devices (Kharrati and Zarrad, 2004).

The radiation spectra are a more complete representation of the X-ray beam, since they provide information about the intensity and energy of the photons (Johns and Cunningham, 1983). Thereby, since the dose depends on the photon energy, the knowledge of the spectral distribution of the beam transmitted by the protective material should be more appropriate for dose assessments of workers and members of the public present in controlled and uncontrolled areas, respectively. In other words, the availability of the energy spectra transmitted by shielding materials allows an better estimation of the absorbed dose (Johns and Cunningham, 1983) for the individuals present in the protected area than the estimations done considering only the air kerma data obtained, for example, from radiation surveys.

A model for shielding calculation which takes into account the influence of the X-ray diagnostic spectra was proposed in 2002 (Costa and Caldas, 2002). This model estimates the attenuation curves of the shielding material in terms of the ambient dose equivalent (mSv) as a function of the thickness of the protective material. These authors applied this model for primary X-ray spectra produced by a semi-empirical model (Costa et al., 2007). Lead was considered as the protective material. The workload distributions observed in some Brazilian X-ray imaging facilities (Mello and Costa, 2007) were adopted, and the energy distribution of the conversion coefficients relating air kerma to ambient dose equivalent (ICRU, 1998) was considered in the calculations.

The adequacy of the protective barrier (radiation protection survey) is usually assessed by estimating the transmission factor ($B(x)$), which is defined as the ratio of the air kerma beyond the barrier to the non-attenuated air kerma at the same distance (NCRP, 2004). When the shielding design goals are represented in units of ambient dose equivalent (mSv), the conversion between these quantities must take into account the complete radiation energy spectra (ICRU, 1998). The inadequate assessment of the shielding adequacy can be avoided by using a model that allows calculating ambient dose equivalent from air kerma by means of the X-ray spectra and conversion coefficients, as a function of thickness of the shielding material.

Therefore, the aim of the present study was to obtain transmission curves by using measured X-ray spectra in terms of ambient dose equivalent and associate these transmitted spectra to workload characteristic of four typical imaging procedures. This work uses a methodology proposed by Costa and Caldas (2002) which was applied for lead. McCaffrey et al. (2007) took a similar approach using transmitted spectra, but for studying shielding garments. Therefore, the application of this methodology for barite mortar and its association of workload distributions is the main innovative purpose of the present work.

2. Materials and methods

The method used in this work for transmission curve calculation was proposed by Costa and Caldas (2002). This method takes into account the influence of the X-ray spectra represented in ambient dose equivalent units (mSv) and also incorporates the workload distribution of the X-ray facility into the calculations. The function, $H^m(10, x_p)$, showed in Eq. (1), represents the primary radiation levels as a function of the kind of shielding material, m, and its thickness, x_p.

$$H^m(10, x_p) = \sum_{V=0}^{V_{max}} \int_0^{Emax} \left(\frac{H_*(10)}{K_{air}}\right)(E) N^V_{p,n}(E) W(V) e^{-\mu m(E) x_p}\, dE \quad (1)$$

In Eq. (1), $(H_*(10)/K_{ar})(E)$ are the coefficients which convert the air kerma (mGy) to ambient dose equivalent (mSv) as a function of the photon energies. These conversion coefficients are provided for monoenergetic photons by ICRU (ICRU, 1998) and they have a strong energy dependence in the diagnostic energy range. $N^V_{p,n}(E)$ represents the primary broad beam spectra measured at a tube potential, V, as a function of the photon energy, E, and normalized by the current–time product (mAs). $W(V)$ represents the workload distribution, $\mu_m(E)$ are the linear attenuation coefficients of the shielding material and V_{max} is the maximum voltage applied for measurements of spectra in the workload distributions.

The transmission factor can be represented by Archer's equation (Archer et al., 1983), as follows:

$$B(x) = \frac{H^m(10, x_p)}{H^m(10, x_p = 0)} = \left[\left(1 + \frac{\beta}{\alpha}\right)e^{\alpha\gamma x_p} - \frac{\beta}{\alpha}\right]^{-1/\gamma} \quad (2)$$

In Eq. (2), α, β and γ are fitting parameters obtained by using a non-linear least-square method, and x_p is the thickness of the attenuating material.

2.1. X-ray spectra measurements

Diagnostic X-ray beams (40–150 kV) were generated by a tungsten target X-ray tube (Philips, model MGC 450) with 3 mm Al additional filtration (HVL=3.51 mm Al in 80 kV). The X-ray spectra were measured using a CdTe spectrometer with a 9 mm^2 sensitive area (Amptek, model XR-100T). This detector includes a tungsten collimator with 1 mm diameter. Air kerma measurements for each tube potential were performed with a 30 cm^3 cylinder ionization chamber (PTW, model TW23361) calibrated against a PTB traceable standard. Fig. 1 presents a scheme of the experimental setup.

The measured spectra were corrected by the response function of the detector using the stripping procedure (Di Castro et al., 1984) implemented using a Matlab program. This procedure takes into account the K-escape, Compton scattering and detector efficiency corrections. The efficiency curve and K-escape fractions were simulated (Tomal et al., 2014) using PENELOPE code (Salvat et al., 2003), while the Compton scattering fraction was estimated (Terini et al., 1999) using the cross sections from XCOM database

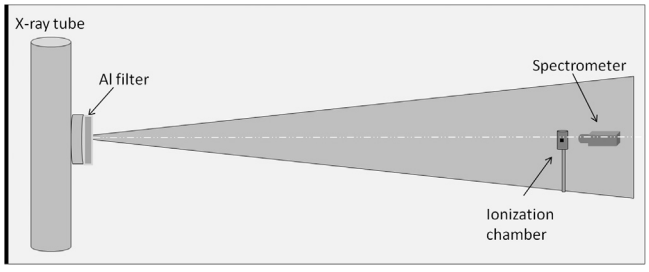

Fig. 1. Experimental setup: positions of devices for air kerma and X-ray spectra measurements. This picture is not in scale.

Table 1
Major compounds found in samples of barite mortar plate and its mass percent.

Major compounds	Mass percent (%)
BaO	33.7
CaO	27.1
SiO_2	14.9
SO_3	14.3
Fe_2O_3	3.16
Al_2O_3	2.85
MgO	1.65

(NIST).

Measurements of air kerma were performed simultaneously along with the X-ray spectra in order to be used as a normalization factor. It was taken into consideration that the area of the corrected spectra is numerically equal to air kerma value obtained with the ion chamber measurements (mGy).

2.2. Calculation input

Transmission curves were calculated using Eq. (1). The workload distribution obtained by Simpkin (1996) for a chest bucky and floor or other barriers, in a radiographic room, and peripheral and cardiac angiography was considered in the calculations. These data are part of workloads distributions determined at 14 US medical institutions and is adopted in the model of NCRP 147 (NCRP, 2004) for shielding calculations in X-ray imaging facilities.

Barite mortar was considered as the shielding material for primary barrier. The chemical composition of the barite mortar was determined by Dispersive X-ray Fluorescence (WDXRF) and fundamental parameter methods (SCAPIN, 2005). The major constituents are presented in Table 1. X-ray mass absorption coefficients for this material were obtained from values provided by database XCOM (NIST) for the compounds found in barite mortar by WDXRF analysis. Fig. 2 shows the X-ray mass absorption coefficients curve for the barite mortar used.

3. Results

Table 2 shows the nominal applied voltage and the corresponding normalized air kerma found from the experimental measurements of the primary spectra. The air kerma values were corrected by air density factor. Fig. 3 shows some primary spectra, from 40 kV to 100 kV in 10 kV steps, measured using the CdTe detector using the technical parameters presented in Table 2 and a 3 mm Al additional filtration.

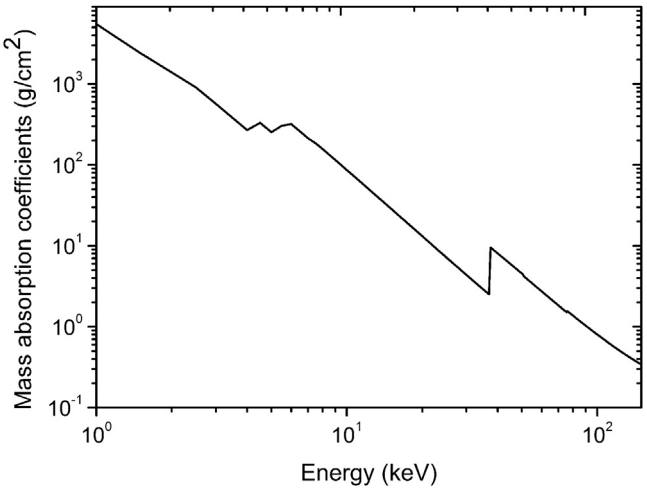

Fig. 2. Mass absorption coefficients curves for the barite mortar obtained from values provided by database XCOM (NIST) for the compounds found in this material by WDXRF analysis.

Table 2
Nominal tube voltage values and corresponding normalized air kerma result for the measured X-ray beams. The air kerma was measured with uncertainty of 1.5%.

Tube voltage (kV)	Normalized air kerma (mGy/mAs)
40	0.010739
50	0.021561
60	0.035761
70	0.050642
80	0.066856
90	0.084736
100	0.099905
110	0.117867
120	0.13744
130	0.137292
140	0.146968
150	0.169042

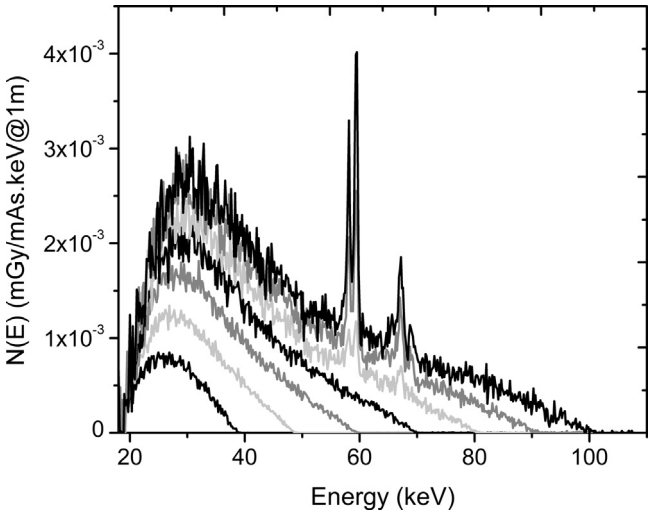

Fig. 3. Experimental primary spectra measured by spectroscopy system with CdTe detector from 40 kV to 100 kV in 10 kV steps.

Primary beam attenuation curves obtained from measured X-ray spectra weighted by different workload distributions and considering the barite mortar mass absorption coefficients are presented in Fig. 4. The results represented by black symbols were calculated using Eq. (1). This calculation takes into account workload distributions for the chest bucky and floor or other barriers, in the radiographic room, and peripheral and cardiac angiography. The X-ray spectra used in this calculation were measured with applied voltages from 40 kV to 150 kV. The curve fittings are presented as solid lines in Fig. 4. The quality of the fittings was evaluated by considering the reduced χ^2 and R^2 parameters. The reduced χ^2 was better than 0.01 and the R^2 was approximately 1 for all fittings.

Table 3 presents the fitting parameters of Archer's model, the non-attenuated ambient dose equivalent, $H^*(10, 0)$, and the HVL corresponding to the curves achieved from the non-linear least squares fitting of Eq. (2) applied on the data points calculated from Eq. (1). The curve fittings are presented as solid lines in Fig. 4.

4. Discussion

The utilization of the optimized model for protective barrier calculation proposed by Costa and Caldas (2002) was generalized

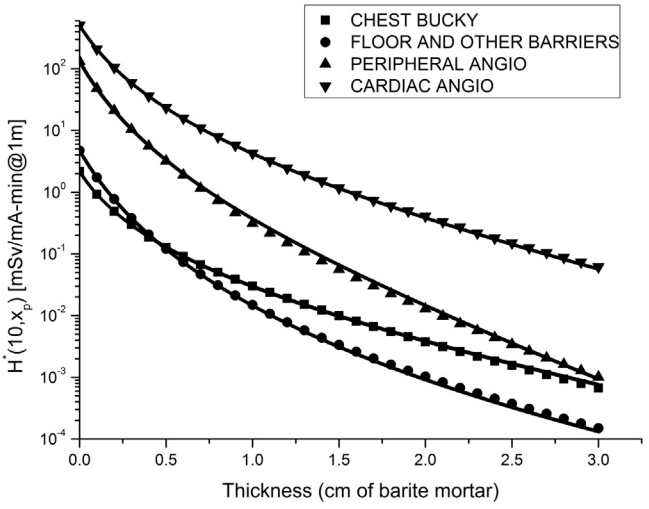

Fig. 4. Attenuation curves provided by barite mortar plates in units of ambient dose equivalent $H^*(10, x_p)$. Different curves consider workload distributions for chest bucky (black squares) and floor or others barriers (black balls), in radiographic room, and peripheral and cardiac angiography.

Table 3
Fitting parameter of Archer's model for attenuation curves of $H^*(10)$, for different workload distributions, as a function of barite mortar thickness and HVL of this distribution.

Parameters	Workload distributions			
	Rad room (chest bucky)	Rad room (floor or other barriers)	Peripheral angio	Cardiac angio
α (cm^{-1})	1.32 (11)	0.8 (7)	2.4 (5)	1.55 (7)
β (cm^{-1})	8.76 (8)	10.3 (7)	9.1 (4)	8.77 (6)
γ	0.474 (13)	0.23 (3)	0.33 (3)	0.40 (1)
$H^*(10,0)$ [mSv/mA min@1 m]	2.1700 (11)	4.706 (3)	132.5 (1)	510.80 (11)
HVL (cm of barite mortar)	0.018 (2)	0.0036 (1)	0.0070 (1)	0.0116 (3)

in the present work including the adoption of directly measured energy spectra and a generic shielding material, the barite mortar. This application shows that the model is adequate for the accurate determination of thickness of shielding material. The results presented in Fig. 4 show the influence of thickness of barite mortar on the beam attenuation. The shapes of the curves are related to the application of the model defined in Eq. (1), which takes into account the primary X-ray spectra in the range of voltages for diagnostic imaging, the workload distribution and the attenuation properties of the shielding material.

From the curves presented in Fig. 4, adequate shielding material thickness for a primary barrier can be determined according to shielding design goals established in units of ambient dose equivalent. The result obtained in the present work for barite mortar as the primary barrier shows qualitative agreement with results found by Costa and Caldas (2002) using lead as protection material and simulated X-ray spectra. Moreover, other authors published results using barite mortar air kerma transmission curves for radiologic energy range using computational methods (Hoff and Firmino, 2007; Hoff et al., 2009) or experimental measurements of transmitted air kerma by an ionizing chamber (Costa and Yoshimura, 2011). The results of these authors also present a good qualitative agreement with the presented results. Quantitative comparisons are not possible since the beam qualities and other experimental conditions are different from those adopted in the present work. Therefore, a user can calculate new transmission curves by just substituting the functions $W(V)$ and $\mu_m(E)$ in Eq. (1).

5. Conclusions

The objective of the study was to apply a previously developed semi-empirical model for calculation of transmission curves of a generic shielding material in units of the quantity ambient dose equivalent. The application was performed using barite mortar linear attenuation coefficient and published workload distributions. Resulting attenuation curves were described in units of ambient dose equivalent ($H^*(10)$). The experimental methodology applied for X-ray measurements using a CdTe detector was considered adequate. It is believed that the consideration of the X-ray spectra in this calculation can yield more realistic and optimized values for shielding of X-ray imaging facilities.

Acknowledgments

The authors thank FAPESP for financial support under project number 2011/04721-9 and research regular project 2010/12237-7, CNPq for support through the project 312029/2009-8 and CNPq/FAPESP funding of project by INCT-Metrology of ionizing radiation in medicine. The authors also thanks Alejandro Gonzales and Daniel Cruz for their contribution on spectra measurements.

References

Akkurt, I., Basyigit, C., Kilincarslan, S., Mavi, B., Akkurt, A., 2006. Radiation shielding of concretes containing different aggregates. Cem. Concr. Comp. 28, 153–157.
Archer, B.R., Fewell, T.R., Conway, B.J., Quinn, P.W., 1994. Attenuation properties of diagnostic x-ray shielding materials. Med. Phys. 21, 1499–1507.
Archer, B.R., Thornby, J.I., Bushong, S.C., 1983. Diagnostic X-ray shielding design based on an empirical model of photon attenuation. Health Phys. 44, 507–517.
Costa, P.R., Caldas, L.V.E., 2002. Evaluation of protective shielding thickness for diagnostic radiology rooms: theory and computer simulation. Med. Phys. 29, 73–85.
Costa, P.R., Nersissian, D.Y., Salvador, F.C., Rio, P.B., Caldas, L.V.E., 2007. Generation of calibrated tungsten target x-ray spectra: modified TBC model. Health Phys. 92, 24–32.
Costa, P.R., Yoshimura, E.M., 2011. Determinação das propriedades de transmissão de argamassas baritadas. Rev. Bras. Fís. Méd. 4, 63–67.
Di Castro, E., Pani, R., Pellegrini, R., Bacci, C., 1984. The use of cadmium telluride detectors for the qualitative analysis of diagnostic x-ray spectra. Phys. Med. Biol. 29, 1117–1131.
Esen, Y., Yilmazer, B., 2010. Investigation of some physical and mechanical properties of concrete produced with barite aggregate. Sci. Res. Essays 5, 3826–3833.
Hoff, G., Firmino, S.F., 2007. Transmission curves to primary beams to diagnostic radiology: a comparison among barite concrete, barite mortar and concrete. IEEE Nucl. Sci. Symp. Conf. Rec. 4, 2587–2591.
Hoff, G., Firmino, S.F., Da Souza, W.P., 2009. Influence of shielding composition on transmission curves determination for diagnostic radiology: a Monte Carlo study using the geant4 code. IEEE Nucl. Sci. Symp. Conf. Rec. 1, 540–543.
IAEA, 2014. Radiation Protection and Safety of Radiation Source: International Basic Safety Standards. IAEA safety standads series, Vienna.
ICRU, 1998. Conversion Coefficients for Use in Radiological Protection against External Radiation. Bethesda, ICRU report 57.
Johns, H.E., Cunningham, J.R., 1983. The Physics of Radiology, fouth edition Thomas Book, Springfield, USA.
Kharrati, H., Zarrad, B., 2004. Computation of conversion coefficients relating air Kerma to Hp(0.07,α), Hp(10,α), and $H^*(10)$ for x-ray narrow spectrum from 40 to 140 kV. Med. Phys. 31, 277–284.
Li, X., Zhang, D., Liu, B., 2012. Transmission of broad W/Rh and W/Al (target/filter) x-ray beams operated at 25–49 kVp through common shielding materials. Med. Phys. 39, 4132–4138.
Ling, T.C., Poon, C.S., Lam, W.S., Chan, T.P., Fung, K.K.L., 2013. X-ray radiation shielding properties of cement mortars prepared with different types of aggregates. Mater. Struct. 46, 1133–1141.
McCaffrey, J.P., Mainegra-Hing, E., Shen, H., 2009. Optimizing non-Pb radiation shielding materials using bilayers. Med. Phys. 36, 5586–5594.
McCaffrey, J.P., Shen, H., Downton, B., Mainegra-Hing, E., 2007. Radiation attenuation by lead and nonlead materials used in radiation shielding garments. Med. Phys. 34, 530–537.

Mello, L.B., Costa, P.R., 2007. Evaluation of workload weighed transmission curves of commercial shielding materials used in diagnostic rooms. In: Proceedings of the International Nuclear Atlantic Conference, Santos, SP.
NCRP, 2004. Structual Shielding Design for Medical X-Ray Imaging Facilities. NCRP report 147 Bethesda, MD.
NIST, [online]. XCOM: Photon Cross Sections Database. ⟨http://physics.nist.gov/PhysRefData/Xcom/html/xcom1.html⟩ (viewed on december 2013).
Okkalides, D., 1991. Assessment of radiology installations in Macedonia, Greece. Eur. J. Radiol. 12, 177–181.
Salvat, F., et. al., 2003. PENELOPE: A Code System for Monte Carlo Simulation of Electron and Photon Transport, Nuclear Energy Agency (NEA), Paris.
Santos, J.C., Costa, P.R., 2014. Evaluation of the effective energy of primary and transmmitted workload weighted X-ray spectra. Radiat. Phys. Chem 95, 221–223.
SCAPIN, A.M., 2005. Validação do método e avaliação da incerteza na determinação de maiores e menores constituintes em solos e sedimentos por WDXRF. In: Procedings of the International Nuclear Atlantic Conference; Encontro Nacional De Aplicações Nucleares. Aben, Santos, São Paulo.
Simpkin, D.J., 1996. Evaluation of NCRP report no. 49 assumptions on workloads and use factors in diagnostic radiology facilities. Med. Phys. 23, 577–584.
Terini, R.A., Costa, P.R., Furquim, T.A.C., Herdade, S.B., 1999. Measurements of discrete and continuous X-ray spectra with a photodiode at room temperature. Appl. Radiat. Isot. 50, 343–353.
Tomal, A., Gonzales, A.H.L., Santos, J.C., Costa, P.R., 2014. Monte Carlo Simulation of the Response Functions of CdTe Detectors to be Applied in X-ray Spectroscopy.